

pubs.acs.org/acssensors Article

Adhesive-Free, Stretchable, and Permeable Multiplex Wound Care Platform

Matthew S. Brown, Karen Browne, Nancy Kirchner, and Ahyeon Koh*



Cite This: ACS Sens. 2022, 7, 1996-2005



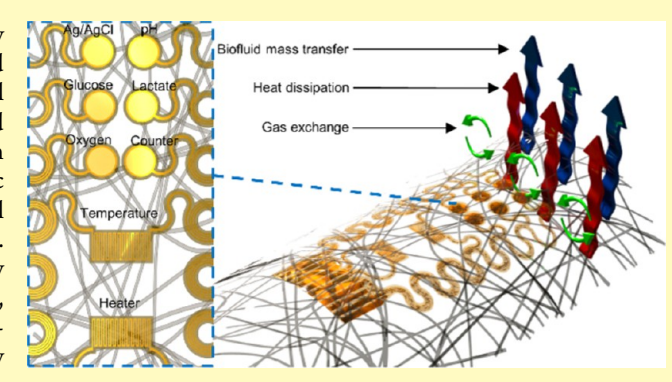
ACCESS I

III Metrics & More

Article Recommendations

Supporting Information

ABSTRACT: The wound healing process remains a poorly understood biological mechanism. The high morbidity and mortality rates associated with chronic wounds are a critical concern to the health care industry. Although assessments and treatment options exist, these strategies have primarily relied on static wound dressings that do not consider the dynamic physicochemical microenvironment and can often create additional complications through the frequent dressing changing procedure. Inspired by the need for engineering "smart" bandages, this study resulted in a multifaceted approach to developing an adhesive-free, permeable, and multiplex sensor system. The electronic-extracellular matrix (e-ECM) platform is capable of noninvasively monitoring chemical and physical changes in real-time on a



flexible, stretchable, and permeable biointegrated platform. The multiplex sensors are constructed atop a soft, thin, and microfibrous substrate of silicone to yield a conformal, adhesive-free, convective, or diffusive wound exudate flow, and passive gas transfer for increased cellular epithelization and unobstructed physical and chemical sensor monitoring at the wound site. This platform emulates the native epidermal mechanics and physical extracellular matrix architecture for intimate bio-integration. The multiple biosensor array can continuously examine inflammatory biomarker such as lactate, glucose, pH, oxygen, and wound temperature that correlates to the wound healing status. Additionally, a heating element was incorporated to maintain the optimal thermal conditions at the wound bed. The e-ECM electrochemical biosensors were tested in vitro, within phosphate-buffered saline, and ex vivo, within wound exudate. The "smart" wound bandage combines biocompatible materials, treatments, and monitoring modalities on a microfibrous platform for complex wound dynamic control and analysis.

KEYWORDS: smart bandage, wound monitoring, multiplex electronics, stretchable electronics, electrochemical sensing, adhesive-free

hronic wound care remains a significant treatment challenge for clinicians and researchers due to a poorly understood and complex repair mechanism. These wounds affect 5.7 million individuals annually, resulting in a cost of \$20 billion.¹⁻³ With the diabetes mellitus diagnosis and the aging population advancing, the number of cases is only expected to rise.² The primary treatment for wound healing relies on wound dressings tailored to address the wound's status; dry or exudative, shallow or deep, and clean or infected.^{4,5} Although advancements in biomaterials are making great strides,6-8 analytical assessment, which is necessary for wound diagnosis and status, is critical to provide precise treatment strategies for chronic wounds. However, clinical wound monitoring and diagnoses require laboratory testing, which is time-consuming, labor-intensive, costly, and incapable of considering the dynamic physicochemical microenvironment, thereby inhibiting wound treatment efficacy. Real-time sensing systems could revolutionize treatment care for chronic wound healing and decrease prolonged hospitalization, doctor visits, expensive laboratory testing, and prolonged antibiotic use.^{4,9}

Recent advances in wearable electronics have revolutionized personal monitoring. These electronics are capable of soft mechanical deformation and seamless integration with soft biological tissue. ^{10–19} Bioelectronics can monitor a broad range of biomarkers quantifying pathophysiological progression, health status, and athletic performance. ^{4,9,11,12,20,21} Most notably, epidermal ^{15,21–23} platforms have brought forth advanced system integrations that allow for a thinner and lighter device capable of conforming to the complex curvilinear structure of the skin establishing an innate, long-term adaptation with the epidermis. Systems of this nature have just started to be translated into clinical application for wound monitoring that could have profound impacts. ^{24–29} However,

Received: April 12, 2022 Accepted: June 23, 2022 Published: July 7, 2022





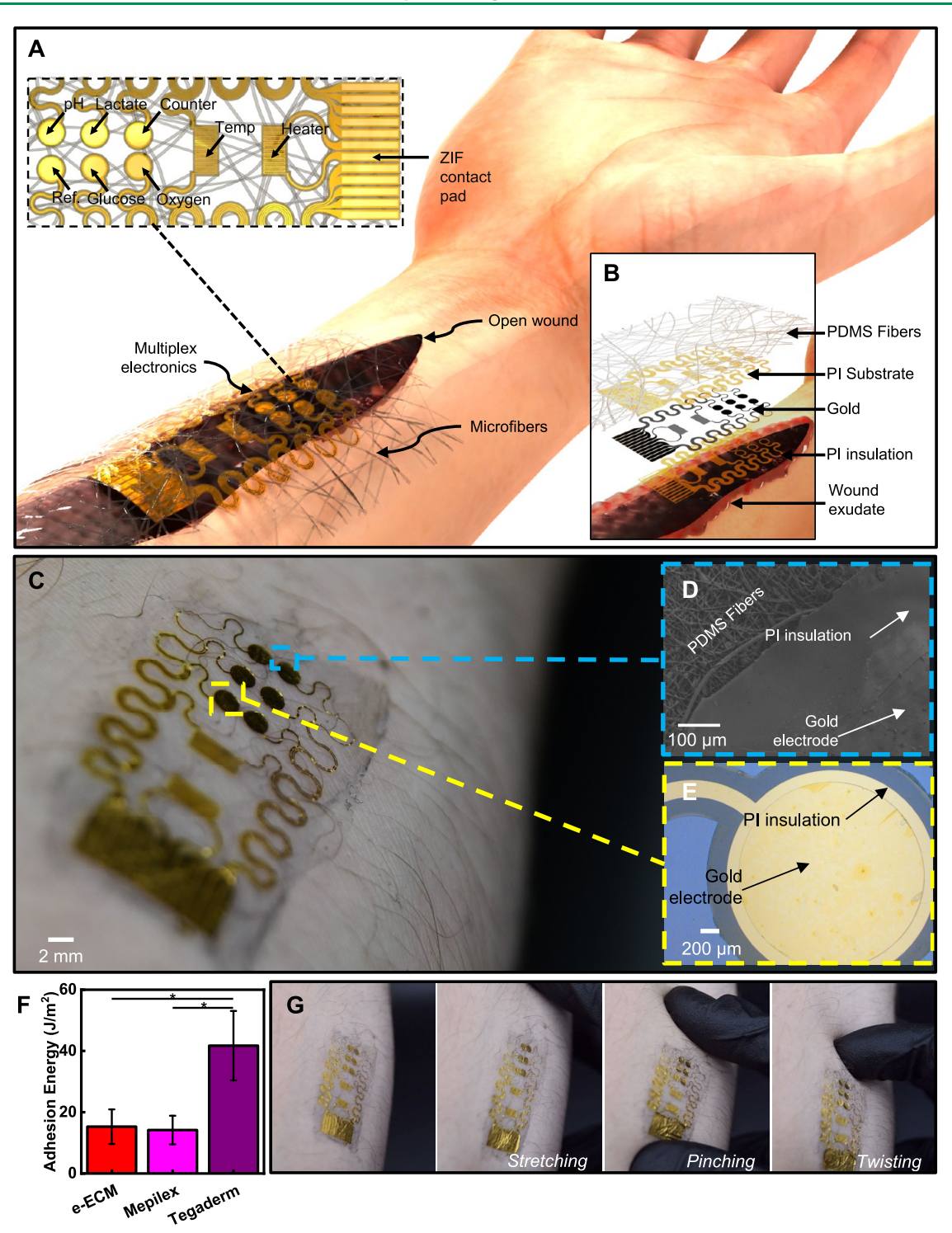


Figure 1. Electronic-extracellular matrix (e-ECM) for inflammation-free chronic wound monitoring. (A) Schematic illustration of e-ECM for chronic wounds and (B) cross-sectional view. (C) Image of e-ECM for chronic wounds. (D) Scanning electron microscope (SEM) image of substrate and electronics. (E) Image of microfabricated electronics. (F) Adhesion energy measured on skin. Mean \pm standard deviation (SD), n = 3, *p < 0.05 Bonferroni correction. (G) Images of e-ECM device under mechanical distortion: stretching, pitching, and twisting.

wound-specific design considerations should be addressed to develop reliable bioelectronics. These platforms should tackle the (1) microspatial mechanical mismatch that exists between rigid electronics and skin, (2) mass transfer of wound exudate, and (3) adhesion while remaining fully biocompatible without disrupting the fragile wound tissue. Reepithelialized tissue is particularly soft and fragile. Skin tissue can be defined between an elastic modulus of E = 10 and 500 kPa. Devices with

similar mechanics can reduce interfacial stress, inflammation, and improve cellular proliferation and migration.³⁰ Although various platforms for on-skin electronics allow for the determination of critical physiological information while imperceptibly integrating with the biological system, these bioelectronics substrates impede the natural diffusive or convective flow of biofluids and gas exchange at the tissue.^{4,24,28,31} Consequently, these drawbacks debilitate the

ACS Sensors pubs.acs.org/acssensors Article

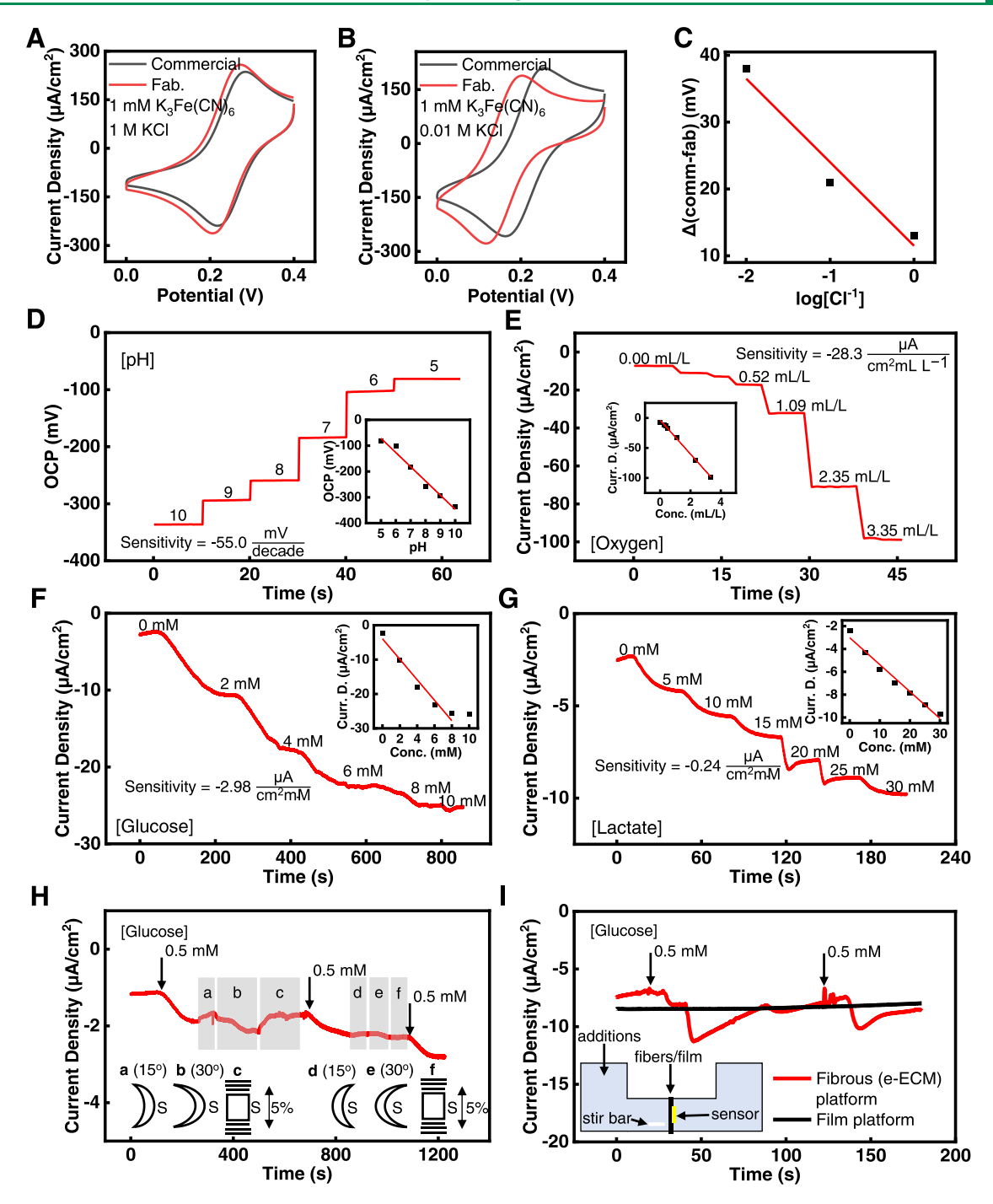


Figure 2. Characteristics of electrochemical sensing in PBS. Cyclic voltammetry performance of fabricated Ag/AgCl reference electrode vs commercial Ag/AgCl (1 M KCl) electrode with (A) 1 M and (B) 0.01 M Cl⁻. (C) Calibration curve of the fabricated reference electrode compared to a commercial Ag/AgCl (1 M KCl) electrode. (D) pH sensor (vs fabricated Ag/AgCl reference electrode) in 37 °C PBS. The inset is the associated calibration curve of the pH sensor. (E) Oxygen, (F) glucose, and (G) lactate sensor (vs fabricated Ag/AgCl reference electrode) in 37 °C PBS (7.4 pH). Insets are the corresponding calibration curves. (H) Electrochemical performance of glucose sensor under mechanical stress (vs fabricated Ag/AgCl reference electrode) in 37 °C PBS (7.4 pH): (a) 15° convex, (b) 30° convex, (c) 5% strain, (d) 15° concave, (e) 30° concave, and (f) 5% strain. (I) Electrochemical performance of glucose sensor on fibrous e-ECM platform vs PDMS film.

devices' ability for wound monitoring, evoking discomfort, tissue inflammation, wound exudate buildup, and delamination, thus disrupting the sensor performance. A fully porous and open-mesh device can overcome these limitations, exhibiting soft mechanics while being fully breathable, allowing the sensor system to directly interact with biofluids while acting invisible to the biological system, not disturbing the physiological environment. In chronic wound care, strong

adhesives have historically been detrimental to the wound bed, creating skin tears and regressing any healing progress.³² Wearable soft bioelectronics are commonly laminated to the skin with commercial adhesives, and adhesive-free alternatives should be explored to reduce skin tears. Forthwith, bioelectronic systems can be developed for long-term applications and multifunctional sensing to improve our quantitative understanding of the dynamic physicochemical

microenvironment and health care devices capable of clinical standards in monitoring biomarker status.

Herein, this study presents the integration of a biomimetic epidermal substrate with multiplex soft bioelectronics, an electronic-extracellular matrix (e-ECM) platform³³ to monitor biomarkers within wound exudate. A soft, adhesive-free, permeable, microfibrous poly(dimethylsiloxane) (PDMS) substrate—physically and mechanically biomimetic to the dermis—was amalgamated with microfabricated biosensors to monitor pH, oxygen, lactate, glucose, and temperature within wound fluid. The device was capable of heat emittance that can be used to improve healing speed. Sensing performance was evaluated within phosphate-buffered saline and compared to conditions within wound exudate derived from a chronic wound. The device performed in the physiological range within wound exudate and upholds a high-performance signal.

■ RESULTS AND DISCUSSION

The configuration for the e-ECM wound care device is presented in Figure 1. The device contains an electrochemical Ag/AgCl reference, counter, and working electrodes for pH, lactate, glucose, and oxygen sensing as well as a temperature sensor and heating coil connected to a 12-pin zero insertion force (ZIF) contact pad. The serpentine-defined units allow for flexibility and biaxial stretchability that connect to a ZIF connector for an external potentiostat. This e-ECM biosensor is developed on a PDMS fibrous mesh with a multiplex electronics array for inflammation-free chronic wound monitoring (Figure 1A—C).

The array consists of six 2 mm diameter electrodes and two coils of 8 mm² with a total thickness of $\approx 5~\mu m$ (polyimide 2 $\mu m/5$ nm Cr/200 nm Au/polyimide 2 μm) (Figure 1B). Fabrication began with photolithographically defining Cr and Au metal deposited by electron beam evaporation on a polyamide (PI) substrate. A second layer of PI encapsulated the Au metal layer except for electrode openings for sensing and the contact pad (Supporting Figure 1). Beneath the PI substrate, the sacrificial layer of poly(methyl methacrylate) (PMMA, 1 μm) was removed by immersing in acetone to retrieve the microfabricated active components onto a water-soluble tape. SiO₂ (50 nm) deposited by electron beam evaporation allowed siloxane bonding to the PDMS fibrous mesh.

In our previous study, the e-ECM platform was fully realized using a coaxial electrospinning fabrication method that was systematically evaluated to produce a microfibrous mesh of PDMS.³³ The developed PDMS matrix (thickness \approx 30 μ m) exhibited soft mechanics ($E = 129.07 \pm 14.85$ kPa) and physical architecture (fiber diameter = 1.99 \pm 0.56 μ m) biomimetic to the dermal extracellular matrix (collagen and elastin fibers).³³ The elastic, fibrous mesh displayed analogous viscoelastic behavior and passive mass transfer of small molecules, transdermal water diffusion, and gas exchange while being fully cytocompatible. Additionally, the platform can maintain adhesive-free lamination and high-resolution biopotential monitoring during vigorous sweating. This PDMS fibrous mesh was fabricated following previous methods and thermally cured.³³ The surface of the mesh was exposed to ultraviolet/ozone to facilitate the siloxane bonding by the activated hydroxyl groups. The sensor array was carefully transferred to covalently bond based on the siloxane chemistry. Dissolving the water-soluble tape removed by immersing in water completed the device fabrication (Figure 1C–E). The eECM device can be laminated onto the skin by van der Waals forces, a fully adhesive-free platform. The adhesion energy presented by the PDMS fibers, $15.27 \pm 5.64 \,\mathrm{J}\,\mathrm{m}^{-1}$ is similar to adhesive-free commercially available wound dressing, Mepilex but presents a statistically significant difference (p < 0.05) to adhesive medical dressing, Tegaderm (Figure 1F). The adhesion strength of the PDMS fibers, $551.74 \pm 203.73 \,\mathrm{kPa}$ was comparable to Tegaderm, and sixfold greater than Mepilex (Supporting Figure 2). The device can remain adhered through commonplace forces presented under stretching, pinching, and twisting (Figure 1G). Forthwith, it can be simply removed with minimal device damage and no skin irritation. This platform can be used as an adhesive-free solution for chronic wound care to prevent skin tears in highrisk patients.

Figure 2 summarizes the analytical performance of the potentiometric, amperometric, and enzymatic electrodes in this type of device construction. The reference and pH electrode were functionalized first to minimize any Ag deposition on the adjacent electrodes. Chronopotentiometry in 0.1 M AgNO₃ produced a conformal Ag film. Linear sweep voltammetry and cyclic voltammetry in 0.1 M KCl and 0.01 M HCl produced nucleation of the AgCl. The reference electrode performance compared to a commercial Ag/AgCl (1 M KCl) reference electrode is shown in Figure 2A-C and Supporting Table 1. As Cl⁻ concentration decreased, the fabricated reference electrode performance deviated with a minor negative potential drift compared to the commercial Ag/AgCl (1 M KCl) electrode (Figure 2C). The reference electrode was able to maintain a stable reference potential throughout a 12-day time period (Supporting Figure 3).

To prepare the pH electrode, Ag/AgCl was electrochemically deposited through the same process as the reference electrode. The ion-selective membrane, H+ ionophore embedded in poly(vinyl chloride) (PVC) coated the Ag/ AgCl layer. Figure 2D illustrates the open-circuit potential (OCP) response of the ion-selective electrode, pH sensor, measured in solutions of 5-10 pH. The voltage response is based on the selective binding of H⁺ ions in solution with the PVC-embedded ionophore. The sensitivity of the sensor, -55.0 mV/decade ($R^2 = 0.98$), for H⁺ ions showed a near-Nernstian cationic slope (Nernstian equation, theoretical sensitivity = 59 mV/decade for ion-selective electrode sensors) within phosphate-buffered saline (PBS) at 37 °C. In a diseased state, chronic wounds can exhibit basic conditions between 7.15 and 8.90 pH, correlating to wound infection. For tissue repair, an acidic environment between 4 and 7 pH is favorable to decrease bacterial viability and improve fibroblast activity.⁴

The amperometric oxygen sensor is based on a Clark-type electrode, an oxygen selective membrane of Nafion and diluted PDMS coated on the oxygen electrode. The outer PDMS membrane improved the electrochemical response to dissolved oxygen. The hydrophobic characteristics of PDMS improved the membrane selectivity. Figure 2E illustrates the chronoamperometric response of the oxygen sensor at $-0.4~\rm V$ vs Ag/AgCl. The sensor could detect a wide range of dissolved oxygen concentrations from 0.00 to 3.35 mL/L dissolved oxygen within PBS (7.4 pH, 37 °C) (Figure 2E). The oxygen sensor could exhibit a sensitivity of $-28.3~\mu A/\rm cm^2$ per mL/L O₂ ($R^2 = 0.99$). In blood, the solubility of oxygen is very low, 0.03 mL/L per 1 mmHg of PO₂, and thus, in normal arterial blood, there is about 3.1 mL/L dissolved oxygen (DO) with a PO₂ of approximately 100 mmHg.^{34,35} In normal blood, a

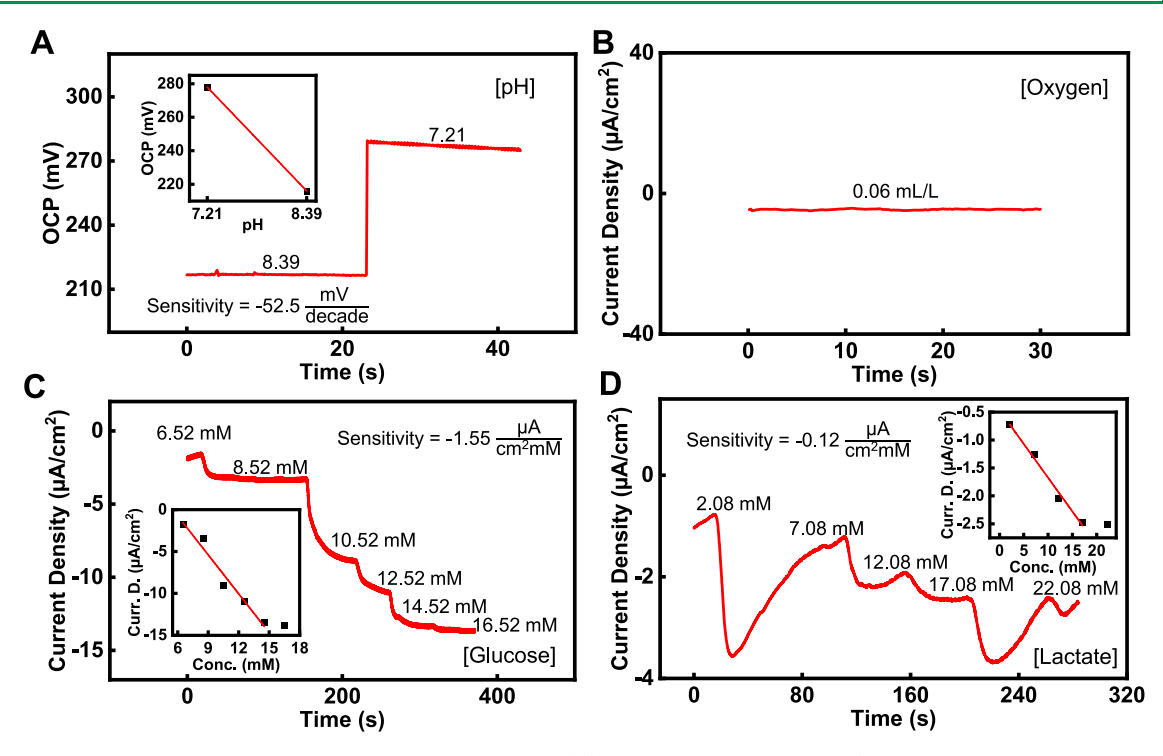


Figure 3. Characteristics of electrochemical sensing in wound exudate. (A) Performance of pH sensor (vs fabricated Ag/AgCl reference electrode) in 37 °C wound exudate. Insets are the corresponding calibration curves. Electrochemical performance of (B) oxygen, (C) glucose, and (D) lactate sensor (vs fabricated Ag/AgCl reference electrode) in 37 °C wound exudate (8.4 pH). Insets are the corresponding calibration curves.

gram of pure hemoglobin can bind with 1.39 mL of oxygen, and when the binding sites of the oxygen capacity are reached (150 g/L hemoglobin), there would be approximately 208.5 mL/L oxygen bound to hemoglobin and around 3.1 mL/L dissolved in the free water of the plasma.³⁵ In other words, the dissolved oxygen in blood accounts for about 1–2% of the total oxygen content with the remaining 98% bound to hemoglobin. For a chronic wound suffering from tissue hypoxia, oxygen therapy can be used to elevate the dissolved oxygen concentration at the wound site.

The enzymatic sensors, glucose and lactate, are based on glucose and lactate oxidase enzymes that are immobilized by a chitosan and single-walled carbon nanotube (SWCNTs) solution on a Prussian Blue mediator layer. After electrochemical cleaning in H₂SO₄, the Prussian Blue mediator layer was electrochemically deposited through cyclic voltammetry (Supporting Figure 4). An applied potential of 0 V vs Ag/AgCl produced the amperometric response for both sensors. Figure 2F presents the glucose response, which produced a linear range of 0-8 mM and sensitivity of -2.98 μ A/cm²mM (R^2 = 0.96). Healthy glucose levels in the blood range from 3.9 to 7.8 mM, while in a chronic wound, high glucose levels can indicate infection and insulin deficiency. Figure 2G presents the lactate response, demonstrating a linear range of 0-30 mM with a sensitivity of $-0.24 \mu \text{A/cm}^2 \text{mM}$ ($R^2 = 0.98$). At a wound, healthy lactate levels range from 1 to 3 mM and concentrations above 7 mM can indicate wound healing impairments.⁴ The selectivity of the glucose and lactate sensor was evaluated against physiological levels of relevant electroactive analytes in the blood (Supporting Figure 5). The sensors can differentiate and express high selectivity for glucose and lactate sensing. The interference current produced by uric acid, ascorbic acid, and potassium chloride was negligible compared to the strong signal response seen with the target analyte. The high selectivity is attributed to the low operating potential from the Prussian Blue mediator layer.

The glucose sensor was subjected to mechanical deformation to evaluate the flexibility and durability of the device construction. The platform underwent changes in structural flexion and tension while submerged in phosphate-buffered saline (7.4 pH) at 37 °C (Figure 2H). Smaller concentrations of glucose, 0.5 mM were added to the solution to illustrate the low current changes to deformation. At convex configuration (Figure 2H(a,b)), the device exhibited a similar large current output. However, when the sensor was stretched at 5% strain uniaxially (Figure 2H(c)), the current stabilized representative of the glucose concentration in solution. The sensor was set back to rest and the current fully stabilized back to 0.5 mM glucose and was able to respond to an addition of 0.5 mM glucose. When concaved (Figure 2H(d,e)), the current response was minimal. Subsequently, with a 5% uniaxial strain (Figure 2H(f)), a minimal signal change was recorded. The device was set back to rest and the current signal was restabilized back to 1 mM glucose. An extra glucose addition of 0.5 mM produced a similar 0.5 mM current response without showing signs of any device damage. In application, the device will undergo concaved configuration and deformation; therefore, the sensors are able to withstand applicable conditions.

To demonstrate the permeability of the platform, the glucose sensor was evaluated within an H-cell. The glucose sensor was laminated on the e-ECM (fibrous) and conventional, PDMS (film) platform. Additions of glucose were added to the far side of the H-cell to evaluate diffusion across the membrane. A stir bar on the far side produced a convection environment, while the glucose diffused across the e-ECM membrane. The glucose additions can be seen in the amperometry response; however, a diffusion-dependent stabilization is present (Figure 2I). As expected, on the film

ACS Sensors pubs.acs.org/acssensors Article

platform (with a similar substrate thickness), a glucose response is undetectable. This has been a critical issue for wearable electronics to detect real-time biomarkers in situ. The proposed device presents the mass transfer of biofluids through the substrate and the diffusion of biomarkers for real-time detection without the risk of analyte accumulation. Additional analysis of permeability is quantified within our previous work. ³⁶

The electrochemical sensors were further characterized within ex vivo wound exudate from a pressure ulcer. At the time the exudate was collected, the patient was suffering an infected stage 4 pressure injury. A detailed explanation of the patient's state is described in the Supporting Information. The electrochemical performance of the e-ECM device within chronic wound exudate is presented in Figure 3 and Supporting Figures 6 and 7. Compared to sensing within PBS, the sensor performance changed and generated a different potential or current response which extended the PBS calibrated conditions. Competitive reactions were observed during cyclic voltammetry and differential pulse voltammetry within wound exudate. The pH electrode was calibrated by a two-point calibration from 8.39-7.21 pH (Figure 3A). The sensitivity of the sensor remained comparable to PBS conditions and behaved based on the Nernst equation (Supporting Figure 7A). However, a positive open-circuit potential drift was observed (~475 mV increase). We suspect the Cl⁻ concentration changes in the solution affected the potential drift since the patient suffered from chronic kidney disease and presented with a severe imbalance of electrolytes. The basic pH presented, 8.39 pH, confirms the patient had an infection. The oxygen sensor presented a low dissolved oxygen concentration of 0.06 mL/L, which also extended the boundaries of the PBS calibration curve (Figure 3B). At an applied potential of -0.4 V vs Ag/AgCl, the amperometric response of the oxygen sensor was recorded. The low dissolved oxygen concentration was suspected to be observed because of the increased viscosity of the solution and low solubility of oxygen in blood 0.03 mL/L per 1 mmHg of PO₂.³⁴ The consistency and composition of wound exudate with respect to both endogenous and exogenous contents vary drastically from patient to patient and over the course of the healing process. ^{37,38} Chronic wound ulcers present a sticky consistency with a high viscosity, protein content (>30 mg/mL), bacterial aggregation, inflammatory cells, and blood leakage. 37,38 Therefore, the high viscosity is suspected to decrease the dissolved oxygen concentration in solution. Additionally, the basic pH along with Cl⁻ changes within the wound exudate is assumed to change the reference potential and oxygen sensor performance (Supporting Figure 8).

The enzymatic glucose and lactate sensor responses are presented in Figure 3C,D. The cyclic and differential pulse voltammetry response between PBS and wound exudate confirms that the Prussian Blue reduction potential changes between solutions (Supporting Figure 9). However, during these tests, interfering biological reactions are occurring, causing side reactions and identification of the reduction potential presents a challenge. The Prussian Blue reduction peak is indistinguishable within wound exudate, and the basic pH is expected to shift the reduction peak potential negatively because of the change in reference potential. The decrease in solution oxygen is also suspected to contribute to the sensor sensitivity decrease because the enzymatic action is based on an oxygen competitive reaction (eq 1).

substrate +
$$O_2 \xrightarrow{\text{oxidase}} \text{product} + H_2O_2$$
 (1)

The unknown glucose and lactate concentration was determined with a colorimetric assay to be 6.52 and 2.08 mM, respectively (Supporting Figure 10). Clinically, glucose levels range from 0.6 to 5.9 mM in wound fluid and 4.6-9.9 mM in serum.³⁹ Lactate concentrations range from 5.4 to 16.7 mM in wound fluid and from 1.3 to 6.5 mM in serum.³⁹ However, these concentration ranges in wound fluid have not been well defined to date and conflicting literature exists. 39,40 We suspect that the wound physiology changes from patient to patient and thus defined concentrations have yet to be established. The ex vivo wound exudate in this study was sanguineous and may explain the metabolite concentrations similar to serum levels. ^{37,38} High lactate and glucose levels can affect cell proliferation and at normal concentrations can be representative of positive healing progression.³⁷ A 0 V vs Ag/ AgCl applied potential for both glucose and lactate sensors were employed to produce the amperometric response. The glucose sensor presented a linear range of 6.52-14.52 mM, sensitivity of $-1.55 \mu A/cm^2 mM$ ($R^2 = 0.96$), and a limit of linearity of 14.52 mM (Figure 3C). The lactate sensor presented a linear range of 2.08-17.08 mM, sensitivity of $-0.12 \,\mu\text{A/cm}^2\text{mM}$ ($R^2 = 0.98$), and a limit of linearity of 17.08 mM (Figure 3D). The limit of linearity increased for both sensors because the minimal oxygen in solution extended the detection range but decreased the sensitivity. The sensitivity of both sensors can be described as a 1:2 ratio of conditions from PBS to wound exudate. The response drift observed from the lactate sensors is suspected to be a diffusion limitation because of the viscous wound exudate. The diffusion limitation appears to minimally affect the glucose sensor compared to the lactate sensor because of the thickness of the biosensing membranes. The glucose sensor is developed on a two-layered system and the lactate is developed on a three-layered membrane construction. Additionally, the detection range observed within wound exudate changes with both the glucose and lactate sensor. In theory, the decrease in available oxygen within the wound exudate should increase the detection range of both sensors; however, this is only observed with the glucose sensor. We suspect the higher pH is negatively affecting the lactate oxidase relative activity. 41 Glucose oxidase can also be affected by an increased pH; however, it generally possesses increased stability compared to lactate oxidase. Based on the output of all electrochemical sensors, in application, the biosensor would require recalibration in wound exudate. Additionally, since wound exudate can vary from the healing stage, as well as patient to patient, calibration would be required frequently to ensure the sensor accuracy with this configuration. The changes in solution viscosity, biofouling, pH, chloride concentration, and solution conductivity are expected to contribute to this performance change. 42,43 Developing applicable sensors would require in situ calibration since laboratory solutions (e.g., PBS) do not present reliable mediums.

After testing in wound exudate, the e-ECM platform was immediately fixed and evaluated. Surface protein aggregation can be observed from the scanning electron microscope (SEM) image of the substrate (Supporting Figure 11A). Energy-dispersive X-ray spectra (EDS) of the proteins were evaluated (Supporting Figure 11B). The nitrogen and sodium peaks seen within the spectrum indicate the presence of nodules that have aggregated onto the PDMS fibers. Their

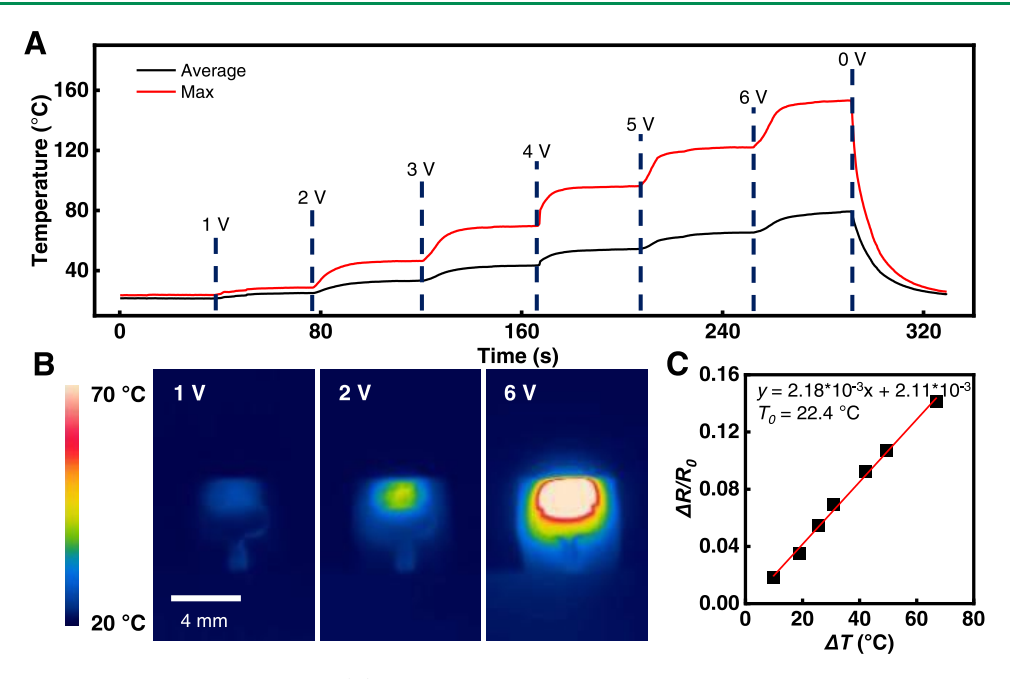


Figure 4. Heater and temperature sensor performance. (A) Temperature evolution of the heater from 1 to 6 V DC bias voltage, captured by an IR camera at corresponding voltages. (B) Thermal profiles emitted from the heater, captured by an IR camera at 1, 2, and 6 V. (C) Calibration curve of the RTD sensor, four-probe resistance vs temperature response of a thermocouple.

presence confirmed that the high protein content in the complex medium can present a potential issue for biofouling. We suspect the immediate fixation with glutaraldehyde increased the protein aggregation onto the surface of the PDMS fibers. Though biofouling can still occur, the porous structure will provide a permeable substrate for the wound exudate to passively permeate. Of note, the substrate is capable of cellular infiltration. The soft and fibrous architecture can facilitate cellular infiltration and maintain viability throughout the fibrous mesh. The soft and fibrous architecture can facilitate cellular infiltration and maintain viability throughout the fibrous mesh.

Maintaining a warm wound bed is vital to ensure optimal healing speeds. 45,46 We demonstrated an electrically driven resistive temperature sensor and heater incorporated into the e-ECM device (Figure 4). The heater was fully insulated with PI to mitigate any interaction with the surrounding biological tissue and wound fluid. The Joule heating properties of the heater are shown in Figure 4A,B. A fixed DC bias voltage was applied with 1 V increments from 1 to 6 V. Captured by an infrared (IR) camera, the temperature generated presented smooth and responsive transitions localized to the heating elements. At 2 V, the heater produced an average heat output of 33.2 °C and a maximum temperature of 46.2 °C. The low voltage demonstrates the efficiency of the resistor. Additional applications can incorporate a drug delivery system atop the heater with a thermoresponsive polymer to elicit a controlled antibiotic or growth factor drug release. Monitoring wound temperature can be used in a clinical setting to access the status of the wound. Decreasing wound bed temperature can be associated with a lack of blood flow. 46,47 A four-probe resistive temperature detector was calibrated with a thermocouple (Figure 4C). The relationship between resistance and temperature is linearly proportional and can be denoted by the following equation

$$R = R_0 (1 + \alpha (T - T_0)) \tag{2}$$

where R is the changed resistances, R_0 is the initial resistance, α is the temperature coefficient of resistance (TCR), T is the

measured temperature, and T_0 is the initial temperature.⁴⁸ The calibration curve presented an R^2 of 0.99 and a TCR of 2.18 × 10^{-3} °C⁻¹ at 22.4 °C. The TCR of gold is 3.70×10^{-3} at 20.0 °C, comparable to the calculated TCR of the temperature sensor.

CONCLUSIONS

We present the development of a soft, permeable, multiplex biosensor capable of adhesive-free lamination for monitoring chronic wounds. This engineering development presents a biomimetic, open-mesh scaffold for transdermal water and gas diffusion, free mass transfer, high adhesion energy, and is capable of mechanical deformation. Siloxane bonding facilitated robust integration with soft electronics and the microfibrous scaffold to develop the e-ECM platform. The electrochemical array delivered simultaneous quantitative assessment of multiple inflammatory biomarkers (pH, oxygen, glucose, lactate, and temperature) within physiologically relevant ranges in a matter of minutes. Testing within wound exudate revealed variations in sensing performance from laboratory-based PBS solution that has not been presented in the literature thus far. Changes in sensor performance can be attributed to solution viscosity, biofouling, changes in pH and chloride concentration, and decrease in available dissolved oxygen. Wound exudated drastically varies from patient to patient and depends on the current patients healing stage and wound status. The development of applicable sensors must be capable of addressing these solution characteristics and recalibrating accordingly.

Ultimately, this platform illustrates a first step toward engineering electrochemical sensors for monitoring wound exudate biomarkers. The porous architecture of this platform permits the ability to monitor analytes in real-time on a biofluid and small molecule permeable substrate. This technology can allow for high-performance sensing that is unperturbed from analyte accumulation and device delaminate that occurs with occlusive platforms which contribute to

wound exudate buildup and inflammation. We foresee future work in (1) analyzing the reversible nature of the sensors, (2) developing appropriate comparisons to PBS and various wound exudate conditions to properly calibrate electrochemical sensors, (3) integration of antibiofouling membranes atop the sensing electrodes, (4) long-term reliability and continuous sensing within wound exudate to characterize sensor stability and lifetime, and (5) influence of patient to patient changes of wound exudate on sensing performance. Additionally, the toxicity of the Ag/AgCl electrode should be evaluated to determine its effects on wound healing. ^{49,50} This fabrication and device integration establishes the framework for wound exudate permeable electronics beyond conventional, impermeable, and rigid electronic systems.

EXPERIMENTAL SECTION

Device Fabrication and Integration. The microfabrication process is illustrated in Supporting Figure 12. The fabrication began by cleaning the 4" silicon wafer with deionized water (DI water) and isopropyl alcohol, followed by a washing cycle in a spin rinse dryer. The wafer was preheated to remove any water from the surface at 150 °C for 3 min. A 2% poly(methyl methacrylate) (PMMA) solution was spin-coated at 500 rpm for 5 s and then ramped to 3,000 rpm for 45 s. The wafer was baked for 90 s at 180 °C and left to cool for 3 min. A polyimide (PI) solution was poured and spun at 100 rpm for 10 s to even out the viscous solution. The PI solution was left to sit on the wafer for 10 min to allow the bubbles to evaporate. Next, the wafer was spin-coated at 1,000 rpm (200 rpm/s ramp) for 25 s and then 3,000 rpm (500 rpm/s ramp) for 40 s. The wafer was let to sit for 3 min and then baked at 90 °C, followed by 120 °C for 3 min. The wafer was hard-baked in a nitrogen gas glove box at 250 °C for 1 h. 50 Å of chromium and 2,000 Å of gold was deposited above the PI layer, respectively by e-beam evaporation. A positive photoresist was deposited, spin-coated at 3,000 rpm for 30 s, and hard-baked for 1 min at 110 °C. Photolithography followed with 2 s of hard contact and 0.7 s of exposure. The wafer was then washed with a developer and washed with DI water. Gold and chromium etchant were used to develop the patterns. An insulation PI layer was spin-coated and hardbaked as described above. 280 Å of chromium was deposited above the PI layer by e-beam evaporation. The photoresist was deposited and developed as described above. Chromium etchant defined the mask. The PI insulation was etched by a reactive ion etching (RIE) cycle of 90 sccm O2 at 300 mTorr and 300 W for 6 min. The remaining chromium was removed in chromium etchant. The wafer was soaked in acetone for 1 h, removing the PMMA layer. The sensors were transferred to water-soluble tape and 500 Å of silicon dioxide (SiO₂) was deposited through e-beam deposition. The electronics and PDMS fibers were placed in a plasma cleaner and exposed to 18 W RF for 30 s with 5:1 nitrogen to oxygen. The electronics were laminated on the PDMS fibers immediately and placed in an oven at 100 °C for 1 h. Finally, the sample was submerged in DI water to remove the water-soluble tape, leaving behind the e-ECM device.

Adhesion Testing. All adhesion tests were performed with a group size of n=3 and a Mark10 tensometer using a 25 N force gauge at a 90° peel and strain rate of 30 mm/s. The force—displacement curve for each sample was plotted and the average force $(F_{\rm avg})$ was calculated at the plateau of the curve. The average force was converted to adhesion strength by $F_{\rm avg}/A$, where A is the area of each sample (thickness and width). The average force was converted to adhesion energy, G, by $G = F_{\rm avg}/W$, where W is the width of each sample. Statistical analysis was conducted in R commander. The mean and standard deviation for each sample was calculated and plotted. An ANOVA test was performed, and a post hoc Bonferroni Correction was employed between groups.

Measurements and Testing. The contact pads from the e-ECM devices were connected with a standard 12-pin ZIF connector. Electrochemical tests were performed with a potentiostat (CH

Instruments, 660E and 1040C) Four-probe temperature measurements were performed by connecting the RTD sensor to a digital multimeter (Keysight, 34460A). Heat map images were captured in real-time by an infrared (IR) camera (ETS320).

Reference Electrode. The reference electrode was fabricated by electrochemically depositing a layer of Ag in 0.1 M AgNO $_3$ at 13 mA/cm 2 for 300 s. Next, the electrode was placed in an electrochemical bath of 0.1 M KCl and 0.01 M HCl for Ag chlorination. Linear sweep voltammetry was performed from open-circuit potential (OCP) to 0.4 V (vs Ag/AgCl (1 M KCl)) at 20 mV/s followed by cyclic voltammetry from 0.1 to 0.4 V vs Ag/AgCl (1 M KCl) at 100 mV/s for 20 cycles.

pH Electrode. The reference electrode fabrication was used for the development of the pH sensor. The Ag/AgCl layer was coated with a pH-sensitive membrane of an H $^+$ ionophore. A 1% (v/v) H $^+$ ionophore I, 0.1 wt % potassium tetrakis(4-chlorophenyl)borate, 10% (v/v) nitrophenyl octyl ether, and 5 wt % poly(vinyl chloride) in tetrahydrofuran was prepared; 3 μ L of solution was drop-cast on the Ag/AgCl electrode. The pH sensor was calibrated against a pH probe (Hanna Instruments, HI2020-01) in PBS and in wound exudate.

Oxygen Electrode. The oxygen sensor was prepared by drop-casting three layers of Nafion at 3 μ L onto the gold electrode. A drying time of an hour was used between layers. A selective diffusion membrane of 30 wt % of PDMS (10:1) in toluene was drop-cast at 3 μ L. The membrane was cured at 60 °C for 1 h. The oxygen sensor was calibrated against a dissolved oxygen probe (Hanna Instruments, HI764080) in PBS and in wound exudate.

Glucose and Lactate Electrode. A solution of chitosan and SWCNTs was prepared by mixing 2% acetic acid and 1% chitosan within DI water and stirred with a magnetic stir bar for 2 h. The SWCNTs were added at 2 mg/mL and water bath sonicated for 30 min. The electrodes were electrochemically cleaned in 100 mM H_2SO_4 from -0.4 to 1.4 V (vs Ag/AgCl (1 M KCl)) at 20 mV/s for 1 cycle. A Prussian Blue mediator layer of 100 mM KCl, 2.5 mM K₃Fe(CN)₆, 2.5 mM FeCl₃, and 100 mM HCl was electrochemically deposited in a fresh solution. The Prussian Blue mediator layer was electrochemically deposited by cyclic voltammetry from -0.5 to 0.6 V (vs Ag/AgCl (1 M KCl)) at 50 mV/s for 10 cycles on both the glucose and lactate electrode. For the glucose electrode, the glucose oxidase solution was prepared by 10 mg mL⁻¹ in PBS (pH 7.4) and added to the chitosan/SWCNT at a ratio of 1:2. The glucose oxidase solution was drop-cast at 3 μ L on the electrode surface and left to dry for 1 h. Next, a layer of chitosan/SWCNT was drop-cast at 3 μ L. For the lactate electrode, a 3 µL solution of chitosan/SWCNT was dropcast and allowed to dry for 1 h. A lactate oxidase solution was prepared by 40 mg mL $^{-1}$ in PBS (pH 7.4) and drop-cast at 2 μ L, followed by drying under ambient conditions for an hour. Finally, another 3 µL layer of chitosan/SWCNT solution was drop-cast onto the electrode and allowed to dry for 1 h. After both glucose and lactate electrodes were functionalized, they were left to dry in the refrigerator overnight. The sensors were calibrated in PBS with known analyte concentrations. The unknown concentration of the target analyte in wound exudate was determined with a colorimetric glucose (Thermo Scientific, TR15421) and lactate (Pointe Scientific, L759650) assay. Within wound exudate, the target analyte was added at known concentrations.

Wound Exudate. The wound exudate was collected from the patient by a vacuum-assisted closure device and deposited within a wound canister without the sanitizer pack. The wound exudate was transferred to centrifuge tubes and stored within a freezer until testing. All in vitro testing took place under a biosafety level II cabinet. The collection and experimental handling of the wound exudate were performed in compliance with protocols that were approved by the Institutional Review Board at Binghamton University.

ASSOCIATED CONTENT

Supporting Information

The Supporting Information is available free of charge at https://pubs.acs.org/doi/10.1021/acssensors.2c00787.

SEM fixation methods, description of the clinical care, current state of the patient, and additional characterization of the device and sensors (PDF)

AUTHOR INFORMATION

Corresponding Author

Ahyeon Koh — Department of Biomedical Engineering, State University of New York at Binghamton, Binghamton, New York 13902, United States; orcid.org/0000-0003-2721-2321; Email: akoh@binghamton.edu

Authors

Matthew S. Brown — Department of Biomedical Engineering, State University of New York at Binghamton, Binghamton, New York 13902, United States; orcid.org/0000-0002-1032-1452

Karen Browne – Decker College of Nursing and Health Sciences, State University of New York at Binghamton, Johnson City, New York 13790, United States; Wound, Ostomy, Continence Inpatient Department, United Health Services Hospital, Johnson City, New York 13790, United States

Nancy Kirchner – Wound, Ostomy, Continence Inpatient Department, United Health Services Hospital, Johnson City, New York 13790, United States; orcid.org/0000-0002-9408-0384

Complete contact information is available at: https://pubs.acs.org/10.1021/acssensors.2c00787

Author Contributions

M.S.B. and A.K. led the development idea and designed the experiments. M.S.B. performed the experiments and wrote the paper. K.B. and N.K. supplied the wound exudate from the patient and contributed to writing. A.K. supervised this work, provided guidance, and assisted in drafting the manuscript as the corresponding author.

Notes

The authors declare no competing financial interest.

ACKNOWLEDGMENTS

General: The authors thank the staff of the Nanofabrication Facilities (NLB) and Analytical and Diagnostics Laboratory (ADL) at Binghamton University for technical support. Funding: This work was supported by the National Science Foundation (ECCS #2020486 & #1920979). The authors acknowledge the support of the Small-Scale Systems Integration and Packaging Center of Excellence (S3IP), BU-UHS Seed Grant Funding, and Start-up funds at SUNY Binghamton.

REFERENCES

- (1) Ochoa, M.; Rahimi, R.; Ziaie, B. Flexible sensors for chronic wound management. *IEEE Rev. Biomed. Eng.* **2014**, *7*, 73–86.
- (2) Järbrink, K.; Ni, G.; Sönnergren, H.; Schmidtchen, A.; Pang, C.; Bajpai, R.; Car, J. The humanistic and economic burden of chronic wounds: a protocol for a systematic review. *Syst. Rev.* **2017**, *6*, No. 15.
- (3) Sen, C. K.; Gordillo, G. M.; Roy, S.; Kirsner, R.; Lambert, L.; Hunt, T. K.; Gottrup, F.; Gurtner, G. C.; Longaker, M. T. Human skin wounds: a major and snowballing threat to public health and the economy. *Wound Repair Regener.* **2009**, *17*, 763–771.
- (4) Brown, M. S.; Ashley, B.; Koh, A. Wearable Technology for Chronic Wound Monitoring: Current Dressings, Advancements, and Future Prospects. *Front. Bioeng. Biotechnol.* **2018**, *6*, No. 47.

- (5) Abrigo, M.; McArthur, S. L.; Kingshott, P. Electrospun Nanofibers as Dressings for Chronic Wound Care: Advances, Challenges, and Future Prospects. *Macromol. Biosci.* **2014**, *14*, 772–792.
- (6) Yu, R.; Zhang, H.; Guo, B. Conductive Biomaterials as Bioactive Wound Dressing for Wound Healing and Skin Tissue Engineering. *Nano-Micro Lett.* **2022**, *14*, No. 1.
- (7) Dong, R.; Guo, B. Smart wound dressings for wound healing. *Nano Today* **2021**, *41*, No. 101290.
- (8) Deng, Z.; Yu, R.; Guo, B. Stimuli-responsive conductive hydrogels: design, properties, and applications. *Mater. Chem. Front.* **2021**, *5*, 2092–2123.
- (9) Wang, C.; Sani, E. S.; Gao, W. Wearable Bioelectronics for Chronic Wound Management. *Adv. Funct. Mater.* **2021**, 32, No. 2111022.
- (10) Heikenfeld, J.; Jajack, A.; Rogers, J.; Gutruf, P.; Tian, L.; Pan, T.; Li, R.; Khine, M.; Kim, J.; Wang, J.; Kim, J. Wearable sensors: modalities, challenges, and prospects. *Lab Chip* **2018**, *18*, 217–248.
- (11) Ray, T. R.; Choi, J.; Bandodkar, A. J.; Krishnan, S.; Gutruf, P.; Tian, L.; Ghaffari, R.; Rogers, J. A. Bio-Integrated Wearable Systems: A Comprehensive Review. *Chem. Rev.* **2019**, *119*, 5461–5533.
- (12) Ray, T.; Choi, J.; Reeder, J.; Lee, S. P.; Aranyosi, A. J.; Ghaffari, R.; Rogers, J. A. Soft, skin-interfaced wearable systems for sports science and analytics. *Curr. Opin. Biomed. Eng.* **2019**, *9*, 47–56.
- (13) Wang, C.; Wang, C.; Huang, Z.; Xu, S. Materials and Structures toward Soft Electronics. *Adv. Mater.* **2018**, *30*, No. 1801368.
- (14) Jang, K.-I.; Han, S. Y.; Xu, S.; Mathewson, K. E.; Zhang, Y.; Jeong, J.-W.; Kim, G.-T.; Webb, R. C.; Lee, J. W.; Dawidczyk, T. J.; Kim, R. H.; Song, Y. M.; Yeo, W.-H.; Kim, S.; Cheng, H.; Rhee, S. I.; Chung, J.; Kim, B.; Chung, H. U.; Lee, D.; Yang, Y.; Cho, M.; Gaspar, J. G.; Carbonari, R.; Fabiani, M.; Gratton, G.; Huang, Y.; Rogers, J. A. Rugged and breathable forms of stretchable electronics with adherent composite substrates for transcutaneous monitoring. *Nat. Commun.* 2014, 5, No. 4779.
- (15) Kim, D.-H.; Lu, N.; Ma, R.; Kim, Y.-S.; Kim, R.-H.; Wang, S.; Wu, J.; Won, S. M.; Tao, H.; Islam, A.; Yu, K. J.; Kim, T.-i.; Chowdhury, R.; Ying, M.; Xu, L.; Li, M.; Chung, H.-J.; Keum, H.; McCormick, M.; Liu, P.; Zhang, Y.-W.; Omenetto, F. G.; Huang, Y.; Coleman, T.; Rogers, J. A. Epidermal Electronics. *Science* **2011**, 333, 838–843.
- (16) Kim, J.; Salvatore, G. A.; Araki, H.; Chiarelli, A. M.; Xie, Z.; Banks, A.; Sheng, X.; Liu, Y.; Lee, J. W.; Jang, K.-I.; Heo, S. Y.; Cho, K.; Luo, H.; Zimmerman, B.; Kim, J.; Yan, L.; Feng, X.; Xu, S.; Fabiani, M.; Gratton, G.; Huang, Y.; Paik, U.; Rogers, J. A. Batteryfree, stretchable optoelectronic systems for wireless optical characterization of the skin. *Sci. Adv.* **2016**, *2*, No. e1600418.
- (17) Lee, H.; Song, C.; Hong, Y. S.; Kim, M. S.; Cho, H. R.; Kang, T.; Shin, K.; Choi, S. H.; Hyeon, T.; Kim, D.-H. Wearable/disposable sweat-based glucose monitoring device with multistage transdermal drug delivery module. *Sci. Adv.* **2017**, *3*, No. e1601314.
- (18) Miyamoto, A.; Lee, S.; Cooray, N. F.; Lee, S.; Mori, M.; Matsuhisa, N.; Jin, H.; Yoda, L.; Yokota, T.; Itoh, A.; Sekino, M.; Kawasaki, H.; Ebihara, T.; Amagai, M.; Someya, T. Inflammation-free, gas-permeable, lightweight, stretchable on-skin electronics with nanomeshes. *Nat. Nanotechnol.* **2017**, *12*, 907–913.
- (19) Lee, S.; Sasaki, D.; Kim, D.; Mori, M.; Yokota, T.; Lee, H.; Park, S.; Fukuda, K.; Sekino, M.; Matsuura, K.; Shimizu, T.; Someya, T. Ultrasoft electronics to monitor dynamically pulsing cardiomyocytes. *Nat. Nanotechnol.* **2019**, *14*, 156–160.
- (20) Liu, Y.; Pharr, M.; Salvatore, G. A. Lab-on-Skin: A Review of Flexible and Stretchable Electronics for Wearable Health Monitoring. *ACS Nano* **2017**, *11*, 9614–9635.
- (21) Windmiller, J. R.; Wang, J. Wearable Electrochemical Sensors and Biosensors: A Review. *Electroanalysis* **2013**, 25, 29–46.
- (22) Kim, D. H.; Ghaffari, R.; Lu, N.; Rogers, J. A. Flexible and stretchable electronics for biointegrated devices. *Annu. Rev. Biomed. Eng.* **2012**, *14*, 113–128.
- (23) Kassal, P.; Kim, J.; Kumar, R.; de Araujo, W. R.; Steinberg, I. M.; Steinberg, M. D.; Wang, J. Smart bandage with wireless

- connectivity for uric acid biosensing as an indicator of wound status. *Electrochem. Commun.* **2015**, *56*, *6*–10.
- (24) Gao, Y.; Nguyen, D. T.; Yeo, T.; Lim, S. B.; Tan, W. X.; Madden, L. E.; Jin, L.; Long, J. Y. K.; Aloweni, F. A. B.; Liew, Y. J. A.; Tan, M. L. L.; Ang, S. Y.; Maniya, S. D. O.; Abdelwahab, I.; Loh, K. P.; Chen, C.-H.; Becker, D. L.; Leavesley, D.; Ho, J. S.; Lim, C. T. A flexible multiplexed immunosensor for point-of-care in situ wound monitoring. *Sci. Adv.* **2021**, *7*, No. eabg9614.
- (25) Mostafalu, P.; Kiaee, G.; Giatsidis, G.; Khalilpour, A.; Nabavinia, M.; Dokmeci, M. R.; Sonkusale, S.; Orgill, D. P.; Tamayol, A.; Khademhosseini, A. A Textile Dressing for Temporal and Dosage Controlled Drug Delivery. *Adv. Funct. Mater.* **2017**, 27, No. 1702399.
- (26) Kiaee, G.; Mostafalu, P.; Samandari, M.; Sonkusale, S. A pH-Mediated Electronic Wound Dressing for Controlled Drug Delivery. *Adv. Healthcare Mater.* **2018**, *7*, No. 1800396.
- (27) Swisher, S. L.; Lin, M. C.; Liao, A.; Leeflang, E. J.; Khan, Y.; Pavinatto, F. J.; Mann, K.; Naujokas, A.; Young, D.; Roy, S.; Harrison, M. R.; Arias, A. C.; Subramanian, V.; Maharbiz, M. M. Impedance sensing device enables early detection of pressure ulcers in vivo. *Nat. Commun.* **2015**, *6*, No. 6575.
- (28) Lou, D.; Pang, Q.; Pei, X.; Dong, S.; Li, S.; Tan, W.-q.; Ma, L. Flexible wound healing system for pro-regeneration, temperature monitoring and infection early warning. *Biosens. Bioelectron.* **2020**, *162*, No. 112275.
- (29) Sharifuzzaman, M.; Chhetry, A.; Zahed, M. A.; Yoon, S. H.; Park, C. I.; Zhang, S.; Barman, S. C.; Sharma, S.; Yoon, H.; Park, J. Y. Smart bandage with integrated multifunctional sensors based on MXene-functionalized porous graphene scaffold for chronic wound care management. *Biosens. Bioelectron.* **2020**, *169*, No. 112637.
- (30) Vining, K. H.; Mooney, D. J. Mechanical forces direct stem cell behaviour in development and regeneration. *Nat. Rev. Mol. Cell Biol.* **2017**, *18*, 728–742.
- (31) Zhao, Y.; Wang, B.; Hojaiji, H.; Wang, Z.; Lin, S.; Yeung, C.; Lin, H.; Nguyen, P.; Chiu, K.; Salahi, K.; Cheng, X.; Tan, J.; Cerrillos, B. A.; Emaminejad, S. A wearable freestanding electrochemical sensing system. *Sci. Adv.* **2020**, *6*, No. eaaz0007.
- (32) LeBlanc, K.; Campbell, K. E.; Wood, E.; Beeckman, D. Best practice recommendations for prevention and management of skin tears in aged skin: an overview. *J. Wound Ostomy Continence Nurs.* **2018**, *45*, 540–542.
- (33) Brown, M. S.; Mendoza, M.; Chavoshnejad, P.; Razavi, M. J.; Mahler, G. J.; Koh, A. Electronic-ECM: A Permeable Microporous Elastomer for an Advanced Bio-Integrated Continuous Sensing Platform. *Adv. Mater. Technol.* **2020**, *5*, No. 2000242.
- (34) Powell, F. L.; Wagner, P. D.; West, J. B. Ventilation, Blood Flow, and Gas Exchange. In *Murray and Nadel's Textbook of Respiratory Medicine*, 6th ed.; Broaddus, V. C.; Mason, R. J.; Ernst, J. D.; King, T. E.; Lazarus, S. C.; Murray, J. F.; Nadel, J. A.; Slutsky, A. S.; Gotway, M. B., Eds.; W.B. Saunders: Philadelphia, 2016; pp 44–75.e3.
- (35) Shander, A.; Napolitano, L. M.; Kaufman, M. Anemia in the Surgical ICU. In *Principles of Adult Surgical Critical Care*,Martin, N. D.; Kaplan, L. J., Eds.; Springer International Publishing: Cham, 2016; pp 295–312.
- (36) Brown, M. S.; Mendoza, M.; Chavoshnejad, P.; Razavi, M. J.; Mahler, G. J.; Koh, A. Electronic-ECM: A Permeable Microporous Elastomer for an Advanced Bio-Integrated Continuous Sensing Platform. *Adv. Mater. Technol.* **2020**, *5*, No. 2000242.
- (37) Löffler, M. W.; Schuster, H.; Bühler, S.; Beckert, S. Wound fluid in diabetic foot ulceration: more than just an undefined soup? *Int. J. Lower Extremity Wounds* **2013**, *12*, 113–129.
- (38) Tickle, J. Wound exudate assessment and management: a challenge for clinicans. *Br. J. Nurs.* **2015**, *24*, S38–S43.
- (39) Trengove, N. J.; Langton, S. R.; Stacey, M. C. Biochemical analysis of wound fluid from nonhealing and healing chronic leg ulcers. *Wound Repair Regen.* **1996**, *4*, 234–239.
- (40) Löffler, M.; Zieker, D.; Weinreich, J.; Löb, S.; Königsrainer, I.; Symons, S.; Bühler, S.; Königsrainer, A.; Northoff, H.; Beckert, S.

- Wound fluid lactate concentration: a helpful marker for diagnosing soft-tissue infection in diabetic foot ulcers? Preliminary findings. *Diabetic Med.* **2011**, *28*, 175–178.
- (41) Toda, A.; Nishiya, Y. Gene Cloning, Purification, and Characterization of a Lactate Oxidase from Lactococcus lactis subsp. cremoris IFO3427. *J. Ferment. Bioeng.* **1998**, *85*, 507–510.
- (42) Lin, P.-H.; Li, B.-R. Antifouling strategies in advanced electrochemical sensors and biosensors. *Analyst* **2020**, *145*, 1110–1120.
- (43) Corrie, S. R.; Coffey, J. W.; Islam, J.; Markey, K. A.; Kendall, M. A. F. Blood, sweat, and tears: developing clinically relevant protein biosensors for integrated body fluid analysis. *Analyst* **2015**, *140*, 4350–4364.
- (44) Liu, N.; Xu, Z.; Morrin, A.; Luo, X. Low fouling strategies for electrochemical biosensors targeting disease biomarkers. *Anal. Methods* **2019**, *11*, 702–711.
- (45) Khan, A. A.; Banwell, P. E.; Bakker, M. C.; Gillespie, P. G.; McGrouther, D. A.; Roberts, A. H. Topical radiant heating in wound healing: an experimental study in a donor site wound model*. *Int. Wound J.* **2004**, *1*, 233–40.
- (46) Dini, V.; Salvo, P.; Janowska, A.; Di Francesco, F.; Barbini, A.; Romanelli, M. Correlation Between Wound Temperature Obtained With an Infrared Camera and Clinical Wound Bed Score in Venous Leg Ulcers. *Wounds* **2015**, *27*, 274–278.
- (47) Gethin, G.; Ivory, J. D.; Sezgin, D.; Muller, H.; O'Connor, G.; Vellinga, A. What is the "normal" wound bed temperature? A scoping review and new hypothesis. *Wound Repair Regen.* **2021**, *29*, 843–847.
- (48) Kang, S. K.; Murphy, R. K.; Hwang, S. W.; Lee, S. M.; Harburg, D. V.; Krueger, N. A.; Shin, J.; Gamble, P.; Cheng, H.; Yu, S.; Liu, Z.; McCall, J. G.; Stephen, M.; Ying, H.; Kim, J.; Park, G.; Webb, R. C.; Lee, C. H.; Chung, S.; Wie, D. S.; Gujar, A. D.; Vemulapalli, B.; Kim, A. H.; Lee, K. M.; Cheng, J.; Huang, Y.; Lee, S. H.; Braun, P. V.; Ray, W. Z.; Rogers, J. A. Bioresorbable silicon electronic sensors for the brain. *Nature* **2016**, *530*, 71–76.
- (49) Zhou, Y.; Chen, R.; He, T.; Xu, K.; Du, D.; Zhao, N.; Cheng, X.; Yang, J.; Shi, H.; Lin, Y. Biomedical Potential of Ultrafine Ag/AgCl Nanoparticles Coated on Graphene with Special Reference to Antimicrobial Performances and Burn Wound Healing. ACS Appl. Mater. Interfaces 2016, 8, 15067–15075.
- (50) Nešporová, K.; Pavlík, V.; Šafránková, B.; Vágnerová, H.; Odráška, P.; Žídek, O.; Císařová, N.; Skoroplyas, S.; Kubala, L.; Velebný, V. Effects of wound dressings containing silver on skin and immune cells. *Sci. Rep.* **2020**, *10*, No. 15216.